Hydrogel-regulated interfacial polymerization: a gateway to effective nanostructure tuning of polyamide nanofiltration membranes

Dong Wang,[a] Na Zhang,[a] Jiaojiao Zhang,[a] Yuyao Qin,[a] Sen Wang,[b] Chuyang Y. Tang,[c] Zhining Wang [a,*]

[a] Shandong Provincial Key Laboratory of Water Pollution Control and Resource Reuse, School of Environmental Science and Engineering, Shandong University, Qingdao 266237, P. R. China

[b] State key laboratory of Microbial Technology, Shandong University, Qingdao 266237, P. R. China

[c] Department of Civil Engineering, The University of Hong Kong, Pokfulam, Hong Kong 999077, P. R. China

[*] Corresponding author: wangzhn@sdu.edu.cn

Highlights:

- Hydrogel intermediate layer was used for nanofiltration membrane preparation.
- The hydrogel layer retarded the diffusion of amine monomers during IP.
- The relation among hydrogel viscosity, amine diffusion and PA thickness was built.
- The optimal NF membrane achieved high water permeability and salt rejection.

Abstract

Controllable interfacial polymerization (IP) is eminently desirable for the preparation of high-performance nanofiltration (NF) membranes to address the worldwide water scarcity. Herein, we report a facile and versatile approach to prepare novel polyamide (PA) NF membranes via a hydrogel-assisted IP process. The piperazine (PIP) diffusion was precisely controlled by tailoring the viscosity of the introduced chitosan/ polyvinyl alcohol (CS/PVA) hydrogel via adjusting the hydrogel composition and crosslinking degree. Due to the synergistic effect of the decreased thickness and improved surface hydrophilicity of the PA layer formed atop hydrogel, the hydrogel-regulated thin film composite (TFC-hg) membrane exhibited a high water permeance of 15.5 L m^{-2} h^{-1} bar^{-1}, which was 2.5 times of that of the control membrane. Meanwhile, the TFC-hg membrane achieved a Na_2SO_4 rejection of 99.1% due to the highly cross-linked PA separation film. This work offers a simple and highly effective strategy for constructing high-performance TFC NF membranes towards efficient water treatment.

Keywords: nanofiltration, interfacial polymerization, hydrogel, monomer diffusion, viscosity

1. Introduction

Nanofiltration (NF) membranes, typically in the forms of polyamide (PA) thin film composite (TFC), have great potential for sustainable fresh water supply via desalination and wastewater reclamation [1, 2]. Typical PA TFC membranes are fabricated via interfacial polymerization (IP) between amine and trimesyol chloride monomer atop the porous substrate [3-5]. Extensive efforts, including the evolvement of aqueous/organic phase [6-8], the innovation of substrate [9-11] and the regulation of interfacial monomer distribution [12, 13], have been devoted to tailor the surface and bulk properties of PA layers and to improve their separation performance. Although tremendous advancements have been achieved, the intrinsic trade-off between permeability and selectivity remains a critical challenge [8, 14, 15].

Hydrogel, a three-dimensional polymeric network with excellent capability of absorbing water molecules [16], show widespread applications in biomedicine, tissue engineering and wastewater treatment due to its excellent biocompatibility, biodegradability and chemical stability [17]. Until now, emerging concept of using hydrogels to control IP process has been implemented into TFC PA membrane fabrication. Hydrogel increases amine storage and acts as an aqueous phase to provide a more effective interface for IP. For example, PA nanofilms synthesized via alginate hydrogel interlayer-assisted-IP exhibited a high water permeability of 27.8 L m^{-2} h^{-1} MPa^{-1} and an excellent salt rejection, which was benefited from the formation of a smooth PA separation layer via reducing the diamine monomers diffusion rate [18]. However, it remains a great challenge to achieve precise control of amine diffusion

through hydrogel-assisted-IP reaction. The mechanism among the physicochemical properties of hydrogels (e.g., viscosity, crosslinking degree), amine diffusion, and the hydrogel-regulated IP process, is still not clearly established and comprehended.

Tuning the diffusion of amine monomers is potentially an effective way to construct uniform PA film with ultrathin thickness, which is highly desired to overcome the ubiquitous trade-off for conventional TFC membranes [19]. Noteworthily, the monomer diffusion can be precisely controlled by tailoring the viscosity of the carrier hydrogel via adjusting the hydrogel composition and crosslinking degree [20, 21]. Herein, we proposed a new approach to fabricate high-performance TFC NF membranes via performing IP reaction atop the surface of chitosan/ polyvinyl alcohol (CS/PVA) hydrogel. The effect of CS/PVA ratio and glutaraldehyde concentration on membrane separation performance was investigated. Furthermore, the relationships between hydrogel viscosity, amine monomer diffusion and polyamide layer formation were analyzed. The simple fabrication process and long-time stability of the novel NF membrane make it as an attractive candidate for scalable production. This work provides deep insights into the role of hydrogel during IP process, paving an important direction for the development of high-performance NF membrane toward a wide range of environmental applications.

2. Experimental

2.1. Materials

Polyether sulfone (PES) microfiltration (MF) membrane with an average pore size of 0.22 μm was provided by Yibo Co., Ltd (China). A commercial Dow Filmtec flat sheet membrane, NF 270, was purchased from Sterlitech (USA). Piperazine (PIP, 99%) and deacetylation chitosan (CS, 90%) were provided by Sinopharm Chemical Reagent Co., Ltd (China). Polyvinyl alcohol (PVA, 98%-99% alcoholysis degree) and trimesoyl chloride (TMC, 98%) were purchased from Macklin Biochemical Co., Ltd. Glutaraldehyde (GA, 25 wt%) aqueous solution and other chemicals were provided by Aladdin Co., Ltd (China).

2.2. Hydrogel preparation

5 g CS was completely dissolved in 100 mL of 5 g/v% acetic acid solution, agitating at room temperature overnight to form CS solution [20]. 10 g PVA was dissolved in 90 mL deionized (DI) water with continuous stirring at 90 °C for 2 h to acquire a PVA solution [21]. Afterwards, a range of CS/PVA blend solutions with several PVA mass ratios of 0 %, 20 %, 40 %, 60 %, 80 % and 100 % were prepared by mixing certain amount of CS and PVA solutions. GA solution was used to crosslink hydrogel precursor and inhibit hydrogel swollen effects.

2.3. Hydrogel characterization

CS/PVA hydrogel was soaked in DI water for 48 h at 25 °C to achieve equilibrium swelling. The weight of the inflatable hydrogel was named as W_e. Then the hydrogel was lyophilized and weighed as W_d. The equilibrium water content of CS/PVA hydrogel

was counted as follows [16]:

$$\text{Equilibrium water content} = (W_e\text{-}W_d)/W_d \quad (1)$$

Rheological properties of the prepared CS/PVA hydrogel were evaluated by the Haake Mars rheometer (Haake Mars III, Germany). For all CS/PVA composite hydrogels, the flow behavior was measured within the shear rate scope of 0.01 to 100 s^{-1}. Frequency sweep experiment was conducted over the frequency range of 0.01 to 10 rad/s with a strain of 1%. The dynamic strain sweep test was carried out within the shear rate scope of 0.01% to 100% at a frequency of 1 Hz [17]. The shear viscosity was measured within the shear rate scope of 0.01 to 100 s^{-1}. The diffusion coefficient (D) of hydrogel can be estimated using the Einstein-Stocks equation [22]:

$$D = kT/6\pi r\eta \quad (2)$$

where k represents Boltzman's constant, T represents temperature, r represents radius of the spherical particle, and η represents viscosity.

Hydrogel samples were stored at -80 °C for overnight and dried in FD-1A-50 lyophilizer (Biocool, Ltd. Beijing, China). The dried samples were coated with a thin gold layer (Sputter Coater, Cressington 108) to improve the conductivity [17]. The surface morphologies of CS/PVA hydrogel were analyzed with scanning electron microscope (SEM, FEI, Quanta 250 FEG).

2.4. Membrane preparation

The PES MF membrane was preserved in DI water for overnight before using as the substrate for TFC membrane preparation. Then, the PES substrate was fixed by circular Plexiglas plate and Teflon frame to ensure that only its surface was coated with

hydrogel. Subsequently, 3 mL CS/PVA solution was poured onto the PES MF membrane and stood for 10 min. The residual CS/PVA solution was cleaned by a rubber roller. Afterwards the freshly prepared GA solution was poured onto the CS/PVA saturated PES membrane for another 10 min for further crosslinking [20]. The residual GA solution was poured off and the crosslinked substrate was air-dried, the CS/PVA hydrogel-modified substrate was formed. To optimize the formation condition of the CS/PVA hydrogel, the CS/PVA ratio and the GA concentration were further investigated. The PES membrane with cross-linked CS/PVA hydrogel was named as PES-hg.

The TFC and TFC-hydrogel membranes were fabricated by IP process on PES or CS/PVA coated PES substrate, respectively. Briefly, the substrate membrane was immersed in 1% w/v PIP/water solution. The excess PIP solution was removed after 2 min. Then, 0.15% w/v TMC/hexane solution was poured onto the substrate and kept 1 min to perform the IP process [23]. The obtained membrane was heated at 60 °C in oven for 5 min. Finally, the NF membrane was immersed in DI water before further test. To optimize the formation conditions of the TFC NF membranes, the different CS/PVA ratios and GA concentrations of CS/PVA hydrogel were investigated, as shown in **Table S1**. For example, the TFC-hydrogel membrane with 60% PVA and 0.50 wt% GA was denoted as TFC-hg membrane.

2.5. Membrane characterization

The chemical structure of the fabricated membranes was measured by Fourier transform infrared spectroscopy (FTIR, Bruker, Tensor 27). SEM was used to test the surface morphologies of the prepared membranes. The root mean square (*RMS*) of the

NF membranes was measured by atomic force microscope (AFM, Veeco MultiMode). Anton Paar SurPASS electrokinetic analyzer was employed to investigate the membrane surface zeta potential. A contact angle measurement instrument (DSA100, Kruss) was used to detect the surface hydrophilicity of the samples, and each of the water contact angle was an average data from five random spots. Transmission electron microscopy (TEM, ZEISS crossbeam 550) was employed to perform the cross-section TEM images. For cross-section TEM analyses, membranes samples were embedded in EPON 812 Yellow Resin, then ultrathin sections (~90 nm) were prepared and mounted onto the cooper grids. The surface chemistry of PES and TFC membranes was characterized by X-ray photoelectron spectroscopy (XPS, ESCALAB 250Xi). The crosslinking degree of the PA layer was calculated using the following equations [24]:

$$Crosslinking\ degree\ (\%) = m/(m+n)\times 100\% \quad (3)$$

where m and n represent the cross-linked and linear part of polyamide structure. Based on the chemical formulas of fully cross-linked ($C_{18}H_{12}N_3O_3$) and fully linear ($C_{15}H_{10}O_4N_2$) polyamide, the theoretical O/N ratio can be represented by [25]:

$$O/N = (3m+4n)/(3m+2n) \quad (4)$$

where m and n were calculated by the value of O/N ratio obtained from the XPS analysis.

2.6. Diffusion rate of PIP

The detection of PIP molecules is limited due to the lack of applicable absorbency in ultra-violet (UV). To investigate the effect of CS/PVA hydrogel on the diffusion rate of PIP, fluorescein isothiocyanate-labeled piperazine (FITC-PIP) was synthesized (**Fig. S1**) [26]. A lab-made U-shaped equipment (**Fig. S2**) was employed to perform the diffusion kinetics experiment. 20 mL 0.5 mg/mL FITC-PIP solution was supplemented

in one side of the equipment. 20 mL n-hexane solution was poured into another side of the equipment. The two solutions were separated by a PES or PES-hg membrane in the U-shaped device. 3 mL of n-hexane near to the membrane surface was collected and ultraviolet spectrometer was used to record the UV-vis spectra to detect the FITC-PIP diffusion rate from the aqueous solution to n-hexane solution. The total diffusion time lasted for 1 min and was recorded every 10 s. According to the fitting straight line of absorbance at 495 nm of FITC-PIP vs. diffused concentration in the hexane phase, the FITC-PIP diffusion rate was calculated by the following equation:

$$k = \Delta c/\Delta t \quad (5)$$

where k represents the FITC-PIP diffusion rate through different substrates, Δc represents the change of FITC-PIP concentration in the n-hexane solution, and Δt represents the diffusion time.

2.7. Molecular dynamic (MD) simulation

To further elucidate the diffusion of PIP molecules towards the organic phase across the hydrogel/hexane interface with/without CS/PVA hydrogel, MD simulation by applying Amorphous module in Materials Studio (Biovia Inc.) A simulation box with periodic boundary conditions in all three dimensions was constructed. For the aqueous system, a cubic simulation box containing 10 PIP molecules and 320 H_2O molecules was constructed. While for the hydrogel system, 2 additional repeat units of CS/PVA molecules were inserted into the above pure water system. The COMPASS force field provided technical support to account for the intermolecular interactions. The remaining simulation parameters were set on the basis of the reported work [27].

After the geometry optimization process of the system, the NVT ensemble followed by the NPT ensemble was applied in calculations for 100 ps with a time step of 1.0 fs. Then, another NVT-MD process was equilibrated for 100 ps and the data was collected for analyzing from the final 100 ps. Every 500 steps output a frame containing the geometry information of PIP molecules. According to the Einstein relationship [27], the diffusion coefficients of PIP molecules in the two systems with or without hydrogel can be estimated from calculating the slopes of the mean square displacement (MSD) curves.

2.8. Membrane performance

NF membrane desalination performance of the obtained membrane was tested by a lab-scale crossflow nanofiltration system with four cells with the effective cell area of 3.125 cm^2. The membrane sample was compressed for half an hour at 6 bar before the measurement of water permeability and salt rejection under 4 bar [28]. The concentration of the feed solution (Na_2SO_4, $MgSO_4$, NaCl or $MgCl_2$) was 2000 ppm. Each experiment was conducted at least three times to ensure the reliability of the results and the average value and standard deviation were calculated based on the three parallel measurements. The water permeability (P) and salt rejection (R) of the NF membranes were calculated by the following equations [23]:

$$P = V/(S \times t \times p) \quad (6)$$

$$R = (C_f - C_p)/C_f \times 100\% \quad (7)$$

where V represents the volume of the permeated solution (L), S stands for the effective membrane area (m^2), t represents the permeation time (h) and p represents the operation

pressure during NF process. C_p and C_f represent the salt concentrations in the permeate and feed solution, respectively.

The water/Na_2SO_4 permselectivity (A/B) was obtained using the following equation [24]:

$$A/B = R/(1-R)(p-\Delta\pi) \quad (8)$$

where $\Delta\pi$ represents the osmotic pressure of the feed solution. A commercial NF membrane (NF 270, Dow Filmtec) was also tested as a reference.

3. Results and discussions

3.1. Membrane Characterization

SEM, AFM and TEM were employed to analyze the morphology and structure of the TFC and TFC-hg NF membranes. As shown in **Fig.1A-1C**, the pristine TFC membrane exhibited a nodular structure with tightly packed spherical particle, which is consistent with the reported literatures [29]. The TFC-hg membrane showed a vermicular surface morphology (**Fig. 1D**). The morphology change might be attributed to the increased viscosity of the CS/PVA hydrogel (**Fig. S3** and **Table S2**) and the resulted retardation of PIP monomer diffusion in the vicinity of the organic boundary [30]. Zhang and co-workers [7] suggested that the difference in the diffusion coefficients of PIP and TMC during a IP reaction could result in a diffusion-driven instability. In the current study, the CS/PVA hydrogel had a strong effect on PIP diffusion as a result of physical obstruction and hydrogen bonds (see the **Section 3.2**), which explained the formation of a rougher membrane. The vermicular structure

increased the *RMS* roughness value from 62.6 (TFC membrane) to 92.0 nm (TFC-hg membrane) (**Fig. 1B** and **1E**). As a result, the surface area of the TFC-hg membrane was 1.3 -fold higher than that of the TFC control membrane (**Fig. 1B**, **1E** and **Table 1**), which is beneficial for improving the membrane water permeability [9, 31].

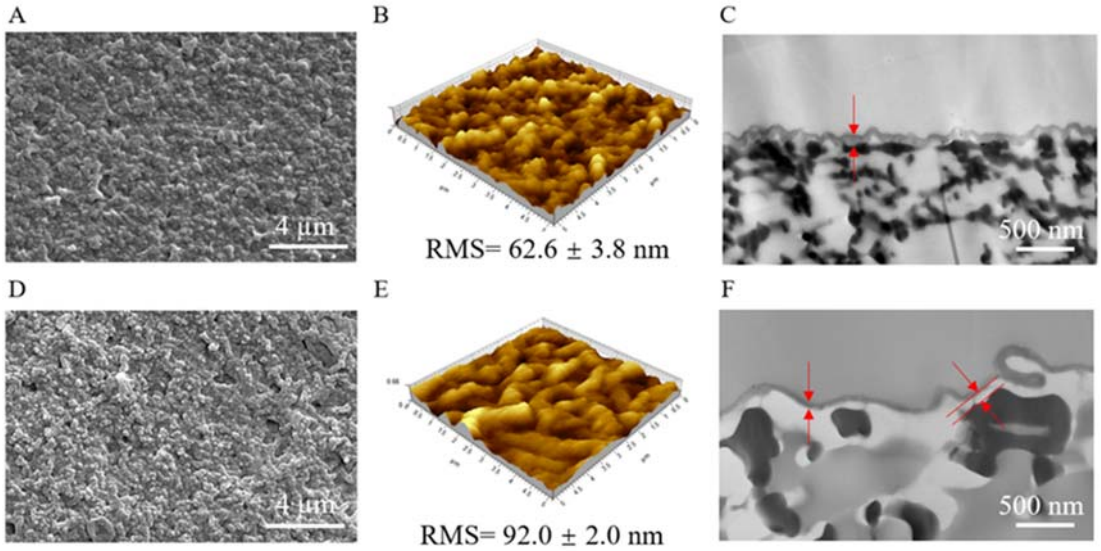

Fig. 1 Top view SEM, AFM, and cross-sectional TEM images of TFC (A, B and C) and TFC-hg membranes (D, E and F).

The cross-sectional TEM features of the TFC and TFC-hg membranes are shown in **Fig 1C** and **1F**, respectively. The thickness of the TFC PA film was approximately 110 nm (**Fig. 1C**). As shown in **Fig. 1F**, there existed an obvious hydrogel intermediate layer (approximately 100 nm) between the vermicular PA nanofilm and the PES substrate. The CS/PVA hydrogel interlayer with a three-dimensional structure could accommodate sufficient PIP monomers to form a complete PA layer [18, 32]. Besides, the PA layer thickness of the TFC-hg significantly decreased to 60 nm due to the

introduction of CS/PVA hydrogel, which could be attributed to the retarded PIP diffusion [32].

Table 1. The surface properties of the fabricated membranes.

Samples	Root mean square roughness (nm)	Surface area (μm^2)	Surface area increase (%)
TFC	62.6 ± 3.8	29.14	16.5 ± 1.2
TFC-hg	92.0 ± 2.0	37.81	51.2 ± 5.7

Surface area increase is calculated according the formula (Sa/Sp -1) × 100%, where Sa and Sp are the actual surface area and the projected area, respectively. Sa is obtained based on the analysis of AFM image using software program Gwyddion 2.51. Sp is acquired from AFM measurements over a scanning area of 5 μm by 5 μm.

To further evaluate the chemical structures of the membranes, the functional groups and element compositions were systematically characterized by FTIR and XPS. From **Fig. 2A**, both TFC and TFC-hg exhibited the distinct polyamide FTIR peak at 1640 cm^{-1}, which could be ascribed to the C=O stretching vibration [33]. In addition, the broad peak at 3400 cm^{-1} of the TFC-hg was attributed to the O−H stretching, suggesting the deposition of CS/PVA hydrogel on the PES substrate [20]. The details of the chemical bonding were acquired by deconvolution of the C 1s, N 1s and O 1s high-resolution XPS spectra (**Fig. 2B-2D**). As shown in **Fig. 2B**, the spectra of the obtained NF membranes manifested different peaks at 531.0, 399.1 and 284.0 eV, which were attributed to O 1s, N 1s and C 1s, respectively [29]. According to **Fig. 2C**, the TFC-hg membrane showed higher unreacted N−H group content (8.60%) than the TFC

membrane, which suggested that more PIP molecules adsorbed onto the PES-hg substrate than that of the PES substrate. As well, the content of O−C=O increased from 15.90% for the TFC control membrane to 21.20% for the TFC-hg membrane (**Fig. 2D**). Sufficient PIP molecules could promote the reaction rate of IP, thus leading to the formation of a highly cross-linked polyamide network. A uniform and dense incipient polyamide layer formed during the initial stage of IP reaction, which in turn restricted the further diffusion of PIP monomers, generating the formation of a thinner PA separation layer (**Fig. 1F**). On account of the retarded diffusion effect, the low PIP contents on the surface of initial PA layer promoted the hydrolysis of TMC, which provided more carboxyl groups and greater hydrophilicity (**Fig. 2D** and **2F**) [11, 34].

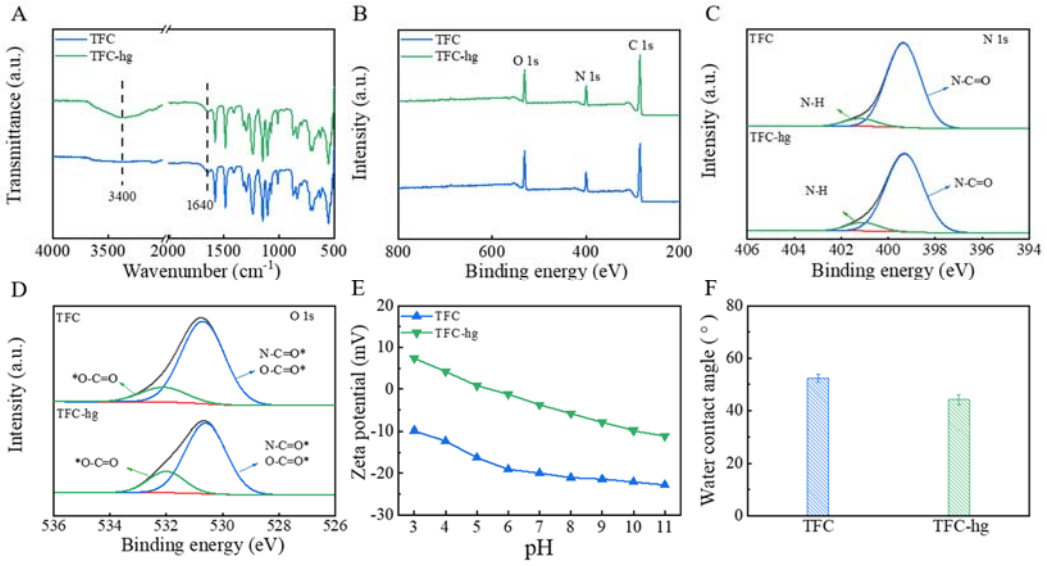

Fig. 2 (A) FTIR, (B) XPS, (C) N 1s spectrum, (D) O 1s spectrum spectra, (E) zeta potential and (F) water contact angle of TFC and TFC-hg membranes.

The crosslinking degree and molecular weight cut-off (MWCO) of TFC and TFC-hg membranes are presented in **Fig. 3**. The abundant PIP monomers could promote the reaction rate of interfacial polymerization, thus leading to the formation of a highly

cross-linked polyamide network. Based on the XPS spectra of N/O element and calculated results using Eq.(3) and (4), the crosslinking degree increased from 72.7% to 85.7% with the introduction of CS/PVA hydrogel, which was beneficial to the improvement of membrane selectivity [29]. Thus, TFC-hg membrane exhibited a smaller MWCO than the TFC membrane (**Fig. 3B**). However, the TFC-hg membrane possessed weak negative surface charge, which ascribed to the synergistic effect of the introduction of CS/PVA hydrogel and carboxyl groups on the membrane surface (**Fig. S4D**) [35].

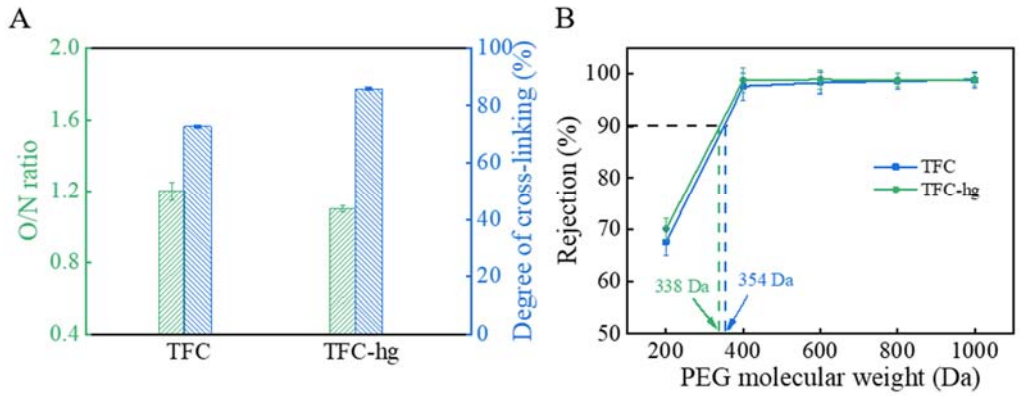

Fig. 3 (A) O/N ratio and crosslinking degree of PA layer and (B) MWCOs of TFC and TFC-hg membranes.

3.2. Mechanism analysis of PIP diffusion

The diffusion of the PIP towards organic phase greatly affects the IP process, hence influences the thickness and morphology of the PA layer. To validate the aqueous monomer diffusion during IP process, the diffusion of PIP was measured using a FITC labeled PIP [26]. As depicted in **Fig. 4A**, the FITC-PIP exhibited a higher diffusion rate in the PES substrate than in the PES-hg substrate. In another words, the cross-linked CS/PVA hydrogel network retarded the diffusion of PIP monomers. MD simulations

were performed to further illuminate the PIP diffusion towards the aqueous/organic phase interface (**Fig. 4B-4D**). The related simulation details were shown in **Fig. S5**. The diffusion coefficients of PIP monomers could be calculated from the curves of the mean square displacement (MSD) in **Fig. 4D**, which was based on the Einstein relationship [29]. The diffusion rate of PIP molecules in water was 7.5 × 10^{-10} m^{-2} s^{-1}, while the diffusion rate of PIP molecules in hydrogel system was 2.4 × 10^{-10} m^{-2} s^{-1}. This result agreed well with the FITC-PIP diffusion experiment, which confirmed that the CS/PVA hydrogel reduced the diffusion rate of PIP molecules. On the one hand, the enlarged viscosity confined the movement of PIP molecules inside the hydrogel. On the other hand, the hydrogen bonding interactions between the CS/PVA hydrogel networks and PIP molecules led to the relatively low PIP diffusion rate, which also affected the IP [27]. Accordingly, an ultrathin PA layer was obtained by the hydrogel-assisted-IP process.

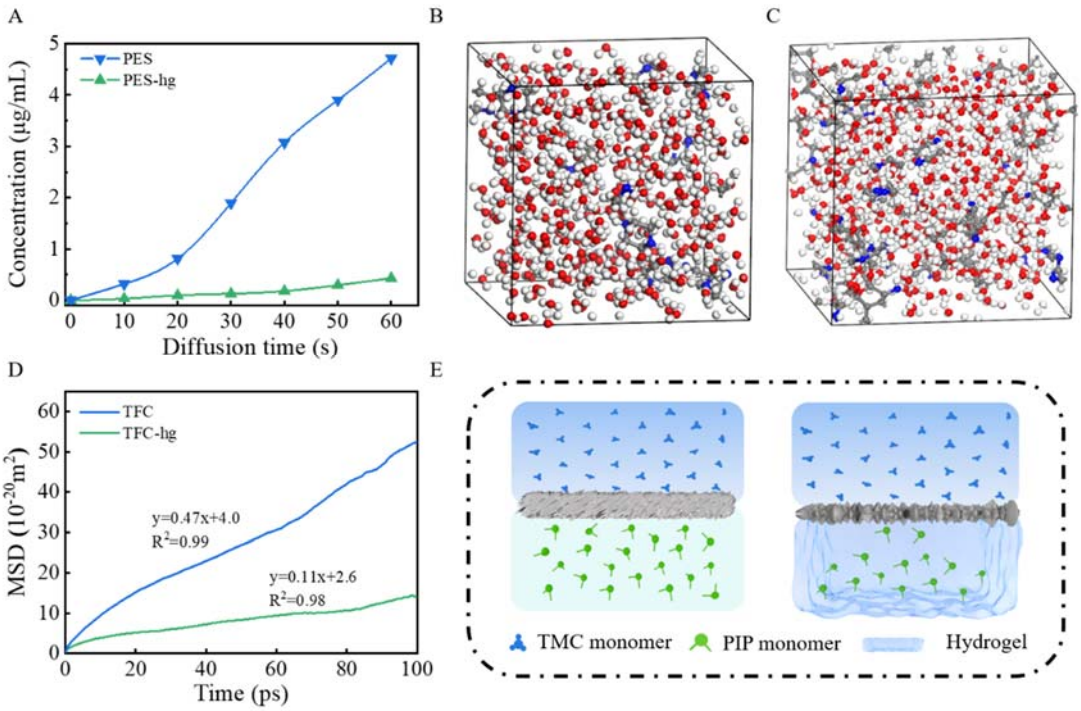

Fig. 4 (A) FITC-PIP diffusion concentration from aqueous phase to organic phase through the PES and PES-hg substrates, MD simulations of PIP molecules in (B) aqueous system and (C) CS/PVA hydrogel, (D) MSD curves of PIP monomers in water and CS/PVA hydrogel systems, and (E) schematical illustrations of the traditional IP process and hydrogel-assisted IP process.

To verify the effect of the hydrogel-regulated IP process on membrane separation performance, the relationship among the hydrogel viscosity, PIP diffusion rate and PA layer thickness was analyzed. As shown in **Fig. 5A** and **5C**, the inverse of viscosity, diffusion rate and PA thickness exhibited similar trend with different hydrogel contents and GA concentrations. The viscosity of the CS/PVA hydrogel increased with increasing CS content (**Fig. S3**). Because the hydroxyl groups in PVA were more likely to form hydrogen bonding, which caused a large steric hindrance effect during aldol reaction [20]. Thus, the hydrogel with higher CS content possessed three-dimensional network structure with higher crosslinking degree [36, 37]. The high-crosslinking hydrogel presented high value of storage modulus (G'), representing a more elastic structure (**Fig. S3**) [36]. Moreover, the stable internal structure increased diffusion resistance, leading to a high viscosity. According to the Einstein-Stocks equation, an inversely proportional remained between diffusion rate and viscosity [38]. Therefore, the PIP diffusion rate reduced with the increase of the hydrogel viscosity. In consequence, the PA thickness reduced from 100 to 50 nm, on account of the retarded diffusion of PIP monomers (**Fig. S6** and **S7**). With the increase of PVA ratio, the O/N ratio gradually decreased and tended to the fixed value (**Table S2** and **S3**), which

indicated a denser PA layer. The molecular weight cut-off (MWCO) of the prepared NF membranes was similar and remarkably consisted with the crosslinking degree of the PA films (**Fig. S8**, **S9** and **Table S3**). Therefore, the water permeability decreased monotonically accompanied with the increase of salt rejection due to the increased thickness (**Fig. 5B**) and crosslinking degree of polyamide layer (**Fig. 3**).

In addition, the TFC NF membranes with different GA concentrations showed the similar results with the above discussions (**Fig. 5C**, **5D** and **Table S4**). The excess GA accelerated the formation of hydrogels and made the hydrogels more compact, which tended to form three-dimensional network structure with higher crosslinking degree and viscosity (**Fig. S10**) [39]. Under the optimal condition, TFC-hg membrane possessed a high water permeability of 15.5 L m^{-2} h^{-1} bar^{-1} accompanied with an excellent Na_2SO_4 rejection of 99.1% (**Fig. 5D**).

To further investigate the viscosity-diffusion rate-PA thickness relationship of TFC-hg membrane, three variables were systematically quantified (**Fig. S12**). The diffusion rate appeared to be strongly dependent on the hydrogel viscosity (correlation coefficient R^2 = 0.99 and 0.94, respectively). Moreover, the PA thickness was also correlated with the diffusion rate. In short, the intercalation of hydrogel layer had a significant impact on the diffusion of amine monomers and properties of polyamide layer, which could regulate IP process and modify the desalination performance of the manufactural TFC NF membranes.

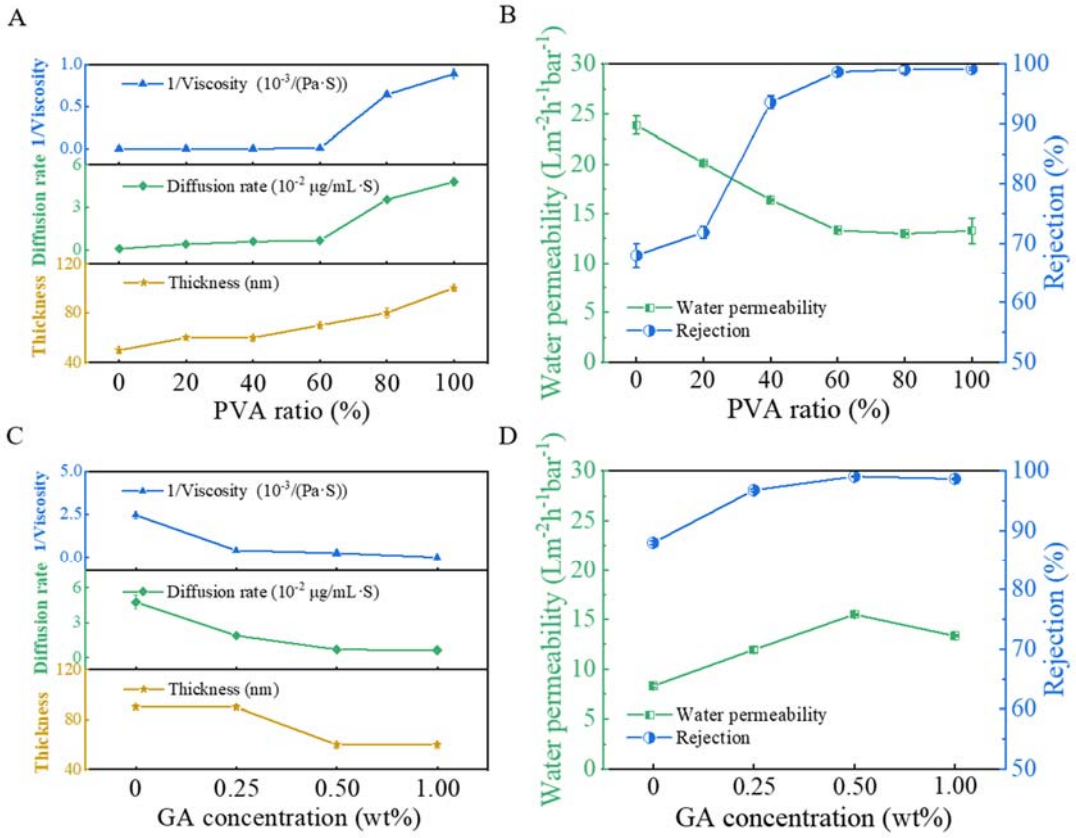

Fig. 5 The relationship diagram of the viscosity, PIP diffusion rate and TEM-apparent with (A) different PVA ratios and (C) GA concentrations, the effect of (B) different PVA ratios and (D) GA concentrations on the NF membrane performance, respectively.

3.3. Membrane performance

Fig. 6A and **6B** exhibit the water permeability and salt rejection of the TFC and TFC-hg membranes. The water permeability of TFC-hg membrane was much higher that of the TFC membrane with four kinds of feed solutions (Na_2SO_4, $MgSO_4$, NaCl and $MgCl_2$) [23]. Combined with the surface properties and cross-sectional structure, the enhanced water permeability was ascribed to the reduced PA thickness, the enhanced surface area and the improved hydrophilicity. Specifically, the reduced thickness of TFC-hg PA layer conduced to shortening of the water molecules transport path. The surface morphology with a vermicular structure provided additional water

transport sites [29]. Based on the solution–diffusion theory, the improved hydrophilicity of the TFC-hg membrane could promote water solubilisation and diffusion through the PA separation layer [40]. The rejection for the four kinds of salt solutions followed the sequence of Na_2SO_4>$MgSO_4$>NaCl >$MgCl_2$, which displayed the typical rejection properties of NF membrane [41]. Both TFC NF membranes presented relatively high rejection of sulfate ions, which was attributed to the synergistic effects of negatively charged and highly crosslinked PA selective layer. Due to Mg^{2+} was prone to shield from negatively charged surface, resulting in higher rejection of sodium salts than magnesium salts [42].

The stability of TFC-hg membranes was investigated under long-term operating conditions (**Fig. 6C**). The TFC-hg membrane maintained a permeability of 15.2 L m^{-2} h^{-1} bar^{-1} and a 99.1% rejection to Na_2SO_4 during 100 h NF operation, which demonstrated the TFC-hg NF membrane possessed excellent stability, benefitting from the enhanced interactions between the hydrogel intermediate layer and the substrate.[19] **Fig. 6D** displays the separation performance of the reported latest NF membranes in terms of water/Na_2SO_4 permselectivity (A/B) and water permeability. The TFC-hg membrane showed outstanding water/salt permselectivity, which lied above the upper bond of the water/Na_2SO_4 selectivity. The superior permselctivity and outstanding stability of the TFC-hg membrane indicated its high potential for practical application in the current water-related treatment.

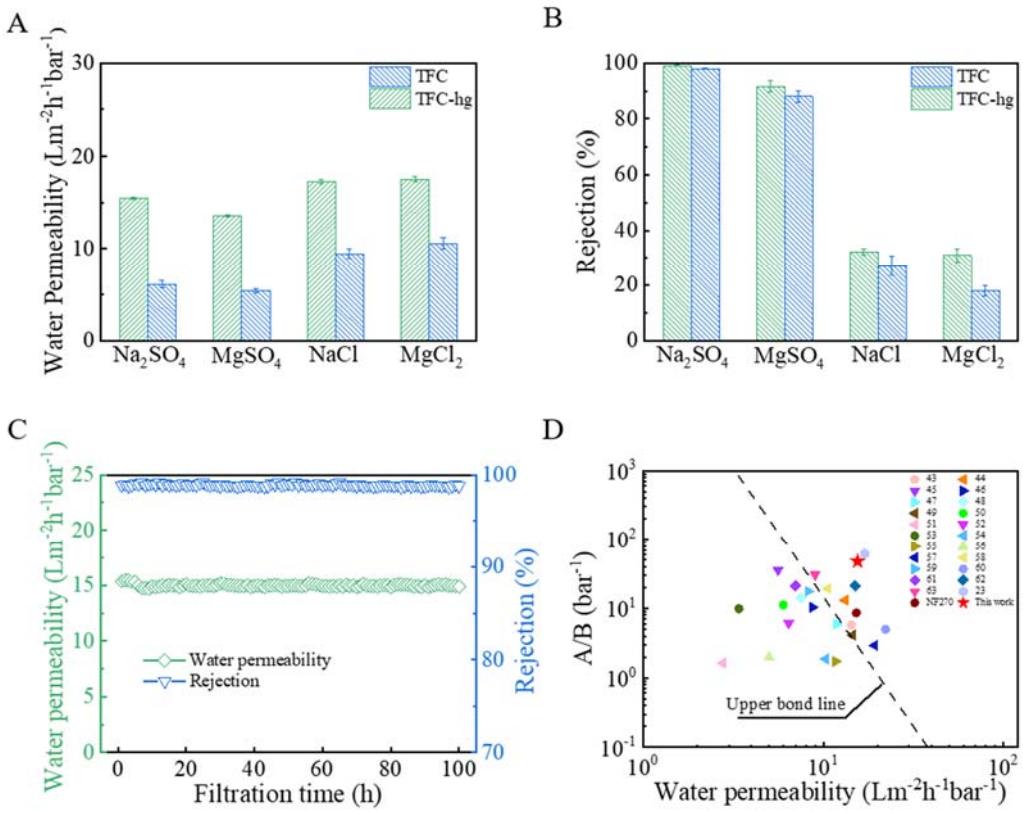

Fig. 6 (A) Water permeability and (B) salt rejection of the TFC and TFC-hg membranes using different inorganic salt solutions as feed, (C) long-term stability of TFC-hg membrane, and (D) water permeability and selectivity of the state-of- the -art NF membranes.[23, 43-63] The upper bond of water/Na_2SO_4 selectivity *A*/*B* was obtained from Ref.[64] copyright (2019).

4. Conclusion

In summary, we fabricated a novel TFC NF membrane via IP process onto the PES support that was modified with CS/PVA hydrogel. Based on the formation and properties of the hydrogels, we systematically investigate the effect of hydrogel viscosity on the diffusion of amine monomers and formation of PA layer. The increased viscosity of hydrogel retarded the diffusion of PIP monomers and decreases the thickness of PA layer, thereby achieving the regulation of IP process and adjustment of

desalination performance of NF membrane. On the basis of the multiple integrations, thinner PA layer, improved membrane hydrophilicity and increased membrane roughness, the optimal TFC-hg NF membrane achieved a water permeability of 15.5 L m^{-2} h^{-1} bar^{-1}, which was 2.5 times as that of the TFC control membrane. In addition, the highly-crosslinked PA layer endowed the TFC-hg membrane with excellent salt rejection (99.1%). This work provides a simple and feasible strategy for fabricating high-performance NF membrane for water desalination.

TOC

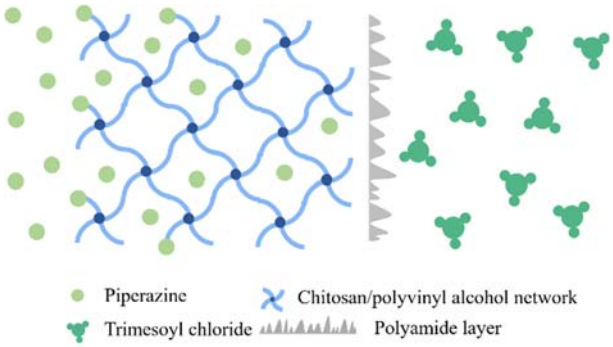

Declaration of Competing Interest

The authors declare no competing financial interest.

Acknowledgements

This work was financially supported by the National Natural Science Foundation of China (22078175), China Postdoctoral Science Foundation (2022M721926), Technological Innovation Projects of Shandong Province (2022CXGC021002), the Natural Science Foundation of Shandong Province (ZR2021LFG010 and ZR2022QB168), and Postdoctoral Innovation Project of Shandong Province (SDCX-ZG-202202021).

References

[1] M.A. Shannon, P.W. Bohn, M. Elimelech, J.G. Georgiadis, B.J. Marinas, A.M. Mayes, Science and technology for water purification in the coming decades, Nature 452(7185) (2008) 301-10. https://doi.org/10.1038/nature06599.

[2] C.Y. Tang, Z. Yang, H. Guo, J.J. Wen, L.D. Nghiem, E. Cornelissen, Potable Water Reuse through Advanced Membrane Technology, Environ. Sci. Technol. 52(18) (2018) 10215-10223. https://doi.org/10.1021/acs.est.8b00562.

[3] L. Zhang, R. Zhang, M. Ji, Y. Lu, Y. Zhu, J. Jin, Polyamide nanofiltration membrane with high mono/divalent salt selectivity via pre-diffusion interfacial polymerization, J. Membr. Sci. 636 (2021) 119478. https://doi.org/10.1016/j.memsci.2021.119478.

[4] S. Cao, A. Deshmukh, L. Wang, Q. Han, Y. Shu, H.Y. Ng, Z. Wang, J.H. Lienhard, Enhancing the Permselectivity of Thin-Film Composite Membranes Interlayered with MoS2 Nanosheets via Precise Thickness Control, Environ. Sci. Technol. 56(12) (2022) 8807-8818. https://doi.org/10.1021/acs.est.2c00551.

[5] P. Sarkar, S. Modak, S. Karan, Ultraselective and Highly Permeable Polyamide Nanofilms for Ionic and Molecular Nanofiltration, Adv. Funct. Mater. 31(3) (2020) 2007054. https://doi.org/10.1002/adfm.202007054.

[6] X. Wei, X. Xu, J. Huang, Z. Wang, H. Li, F. Shao, Z. Guo, Q. Zhou, J. Chen, B. Pan, Optimizing the surface properties of nanofiltration membrane by tailoring the diffusion coefficient of amine monomer, J. Membr. Sci. 656 (2022) 120601. https://doi.org/10.1016/j.memsci.2022.120601.

[7] Z. Tan, S. Chen, X. Peng, L. Zhang, C. Gao, Polyamide membranes with nanoscale

Turing structures for water purification, Science 360 (2018) 518-521. https://doi.org/10.1126/science.aar6308

[8] X. Cheng, C. Lai, J. Li, W. Zhou, X. Zhu, Z. Wang, J. Ding, X. Zhang, D. Wu, H. Liang, C. Zhao, Toward Enhancing Desalination and Heavy Metal Removal of TFC Nanofiltration Membranes: A Cost-Effective Interface Temperature-Regulated Interfacial Polymerization, ACS Appl. Mater. Interfaces 13(48) (2021) 57998-58010. https://doi.org/10.1021/acsami.1c17783.

[9] D. Wang, J. Li, B. Gao, Y. Chen, Z. Wang, Triple-layered thin film nanocomposite membrane toward enhanced forward osmosis performance, J. Membr. Sci. 620 (2021) 118879. https://doi.org/10.1016/j.memsci.2020.118879.

[10] X. Wu, M. Ding, H. Xu, W. Yang, K. Zhang, H. Tian, H. Wang, Z. Xie, Scalable $Ti_3C_2T_x$ MXene Interlayered Forward Osmosis Membranes for Enhanced Water Purification and Organic Solvent Recovery, ACS Nano 14(7) (2020) 9125-9135. https://doi.org/10.1021/acsnano.0c04471.

[11] X. Zhu, X. Cheng, X. Luo, Y. Liu, D. Xu, X. Tang, Z. Gan, L. Yang, G. Li, H. Liang, Ultrathin Thin-Film Composite Polyamide Membranes Constructed on Hydrophilic Poly(vinyl alcohol) Decorated Support Toward Enhanced Nanofiltration Performance, Environ. Sci. Technol. 54(10) (2020) 6365-6374. https://doi.org/10.1021/acs.est.9b06779.

[12] Y. Liang, Y. Zhu, C. Liu, K.R. Lee, W.S. Hung, Z. Wang, Y. Li, M. Elimelech, J. Jin, S. Lin, Polyamide nanofiltration membrane with highly uniform sub-nanometre pores for sub-1 A precision separation, Nat. Commun. 11(1) (2020) 2015.

https://doi.org/10.1038/s41467-020-15771-2.

[13] S.-J. Xu, Q. Shen, L.-H. Luo, Y.-H. Tong, Y.-Z. Wu, Z.-L. Xu, H.-Z. Zhang, Surfactants attached thin film composite (TFC) nanofiltration (NF) membrane via intermolecular interaction for heavy metals removal, J. Membr. Sci. 642 (2022) 119930. https://doi.org/10.1016/j.memsci.2021.119930.

[14] Z. Gu, S. Yu, J. Zhu, P. Li, X. Gao, R. Zhang, Incorporation of lysine-modified UiO-66 for the construction of thin-film nanocomposite nanofiltration membrane with enhanced water flux and salt selectivity, Desalination 493 (2020) 114661. https://doi.org/10.1016/j.desal.2020.114661.

[15] D. Zhou, L. Zhu, Y. Fu, M. Zhu, L. Xue, Development of lower cost seawater desalination processes using nanofiltration technologies — A review, Desalination 376 (2015) 109-116. https://doi.org/10.1016/j.desal.2015.08.020.

[16] W. Zhao, X. Jin, Y. Cong, Y. Liu, J. Fu, Degradable natural polymer hydrogels for articular cartilage tissue engineering, J. Chem. Technol. Biot. 88(3) (2013) 327-339. https://doi.org/10.1002/jctb.3970.

[17] Z. Wang, Y. Zhang, Y. Yin, J. Liu, P. Li, Y. Zhao, D. Bai, H. Zhao, X. Han, Q. Chen, High-Strength and Injectable Supramolecular Hydrogel Self-Assembled by Monomeric Nucleoside for Tooth-Extraction Wound Healing, Adv. Mater. 34(13) (2022) 2108300. https://doi.org/10.1002/adma.202108300.

[18] X. Cheng, Y. Peng, S. Li, B. Su, Alginate hydrogel interlayer assisted interfacial polymerization for enhancing the separation performance of reverse osmosis membrane, J. Membr. Sci. 638 (2021) 119680. https://doi.org/10.1016/j.memsci.2021.119680.

[19] R. Dai, J. Li, Z. Wang, Constructing interlayer to tailor structure and performance of thin-film composite polyamide membranes: A review, Adv. Colloid Interfac. 282 (2020) 102204. https://doi.org/10.1016/j.cis.2020.102204.

[20] P.-I. Cheng, P.-D. Hong, K.-R. Lee, J.-Y. Lai, Y.-L. Tsai, High permselectivity of networked PVA/GA/CS-Ag^{+}-membrane for dehydration of Isopropanol, J. Membr. Sci. 564 (2018) 926-934. https://doi.org/10.1016/j.memsci.2018.06.019.

[21] Y. Zhang, M. Jiang, Y. Zhang, Q. Cao, X. Wang, Y. Han, G. Sun, Y. Li, J. Zhou, Novel lignin-chitosan-PVA composite hydrogel for wound dressing, Mater. Sci. Eng. C Mater. Biol. Appl. 04 (2019) 110002. https://doi.org/10.1016/j.msec.2019.110002.

[22] A. Olejnik, G. Schroeder, I. Nowak, The tetrapeptide N-acetyl-Pro-Pro-Tyr-Leu in skin care formulations-Physicochemical and release studies, Int. J. Pharm. 492(1-2) (2015) 161-8. https://doi.org/10.1016/j.ijpharm.2015.06.050.

[23] H. Lan, P. Li, H. Wang, M. Wang, C. Jiang, Y. Hou, P. Li, Q. Jason Niu, Construction of a gelatin scaffold with water channels for preparing a high performance nanofiltration membrane, Sep. Purif. Technol. 264 (2021) 118391. https://doi.org/10.1016/j.seppur.2021.118391.

[24] Z.-Y. Ma, Y.-R. Xue, Z.-K. Xu, Alginate Hydrogel Assisted Controllable Interfacial Polymerization for High-Performance Nanofiltration Membranes, Membranes 11(6) (2021) 435. https://doi.org/10.3390/membranes11060435.

[25] B. Khorshidi, T. Thundat, B.A. Fleck, M. Sadrzadeh, Thin film composite polyamide membranes: parametric study on the influence of synthesis conditions, RSC Adv. 5(68) (2015) 54985-54997. https://doi.org/10.1039/c5ra08317f.

[26] X. Yang, Controllable Interfacial Polymerization for Nanofiltration Membrane Performance Improvement by the Polyphenol Interlayer, ACS Omega 4(9) (2019) 13824-13833. https://doi.org/10.1021/acsomega.9b01446.

[27] S. Yuan, G. Zhang, J. Zhu, N. Mamrol, S. Liu, Z. Mai, P. Van Puyvelde, B. Van der Bruggen, Hydrogel assisted interfacial polymerization for advanced nanofiltration membranes, J. Mater. Chem. A 8(6) (2020) 3238-3245. https://doi.org/10.1039/c9ta12984g.

[28] S. Li, B. Gao, Y. Wang, B. Jin, Q. Yue, Z. Wang, Antibacterial thin film nanocomposite reverse osmosis membrane by doping silver phosphate loaded graphene oxide quantum dots in polyamide layer, Desalination 464 (2019) 94-104. https://doi.org/10.1016/j.desal.2019.04.029.

[29] S. Han, Z. Mai, Z. Wang, X. Zhang, J. Zhu, J. Shen, J. Wang, Y. Wang, Y. Zhang, Covalent Organic Framework-Mediated Thin-Film Composite Polyamide Membranes toward Precise Ion Sieving, ACS Appl. Mater. Interfaces 14(2) (2022) 3427-3436. https://doi.org/10.1021/acsami.1c19605.

[30] M.J. Tang, M.L. Liu, D.A. Wang, D.D. Shao, H.J. Wang, Z. Cui, X.L. Cao, S.P. Sun, Precisely Patterned Nanostrand Surface of Cucurbituril[n]-Based Nanofiltration Membranes for Effective Alcohol-Water Condensation, Nano Lett. 20(4) (2020) 2717-2723. https://doi.org/10.1021/acs.nanolett.0c00344.

[31] S. Shao, F. Zeng, L. Long, X. Zhu, L.E. Peng, F. Wang, Z. Yang, C.Y. Tang, Nanofiltration Membranes with Crumpled Polyamide Films: A Critical Review on Mechanisms, Performances, and Environmental Applications, Environ. Sci. Technol.

56(18) (2022) 12811-12827. https://doi.org/10.1021/acs.est.2c04736.

[32] Z. Yang, P.F. Sun, X. Li, B. Gan, L. Wang, X. Song, H.D. Park, C.Y. Tang, A Critical Review on Thin-Film Nanocomposite Membranes with Interlayered Structure: Mechanisms, Recent Developments, and Environmental Applications, Environ. Sci. Technol. 54(24) (2020) 15563-15583. https://doi.org/10.1021/acs.est.0c05377.

[33] N. Zhang, X. Song, Y. Chen, B. Jiang, L. Zhang, H. Jiang, A facile and economic route assisted by trace tannic acid to construct a high-performance thin film composite NF membrane for desalination, Environ. Sci. Water Res. Technol. 7(5) (2021) 956-968. https://doi.org/10.1039/d1ew00071c.

[34] C. Jiang, L. Tian, Z. Zhai, Y. Shen, W. Dong, M. He, Y. Hou, Q.J. Niu, Thin-film composite membranes with aqueous template-induced surface nanostructures for enhanced nanofiltration, J. Membr. Sci. 589 (2019) 117244. https://doi.org/10.1016/j.memsci.2019.117244.

[35] Y. Hao, Q. Li, B. He, B. Liao, X. Li, M. Hu, Y. Ji, Z. Cui, M. Younas, J. Li, An ultrahighly permeable-selective nanofiltration membrane mediated by an in situ formed interlayer, J. Mater. Chem. A 8(10) (2020) 5275-5283. https://doi.org/10.1039/c9ta12258c.

[36] Z. Fan, P. Cheng, Y. Gao, D. Wang, G. Jia, P. Zhang, S. Prakash, Z. Wang, J. Han, Understanding the rheological properties of a novel composite salecan/gellan hydrogels, Food Hydrocolloids 123 (2022) 107162. https://doi.org/10.1016/j.foodhyd.2021.107162.

[37] J.H. Chen, X.F. Dong, Y.S. He, Investigation into glutaraldehyde crosslinked

chitosan/cardo-poly-etherketone composite membrane for pervaporation separation of methanol and dimethyl carbonate mixtures, RSC Adv. 6(65) (2016) 60765-60772. https://doi.org/10.1039/c6ra10854g.

[38] M. M. Zgoda, J. Kołodziejska, M. Nachajski, Viscosity of hydrogel pharmaceutical products and the rate of diffusion of ibuprofen hydrotropic binding through model phase boundary in vitro. Polimery w Medycynie 2007,1

[39] C. Xu, W. Zhan, X. Tang, F. Mo, L. Fu, B. Lin, Self-healing chitosan/vanillin hydrogels based on Schiff-base bond/hydrogen bond hybrid linkages, Polym. Test. 66 (2018) 155-163. https://doi.org/10.1016/j.polymertesting.2018.01.016.

[40] X. Gao, Y. Li, X. Yang, Y. Shang, Y. Wang, B. Gao, Z. Wang, Highly permeable and antifouling reverse osmosis membranes with acidified graphitic carbon nitride nanosheets as nanofillers, J. Mater. Chem. A 5(37) (2017) 19875-19883. https://doi.org/10.1039/c7ta06348b.

[41] C. Geng, P. Huang, F. Zhao, H. Dong, H. Niu, Y. Zhou, J. Shen, J. Zhang, Enhancing the long-term separation stability of TFC membrane by the covalent bond between synthetic amino-substituted polyethersulfone substrate and polyamide layer, J. Membr. Sci. 637 (2021) 119637. https://doi.org/10.1016/j.memsci.2021.119637.

[42] L. Shen, R. Cheng, M. Yi, W.S. Hung, S. Japip, L. Tian, X. Zhang, S. Jiang, S. Li, Y. Wang, Polyamide-based membranes with structural homogeneity for ultrafast molecular sieving, Nat. Commun. 13(1) (2022) 500. https://doi.org/10.1038/s41467-022-28183-1.

[43] J. Zhu, L. Qin, A. Uliana, J. Hou, J. Wang, Y. Zhang, X. Li, S. Yuan, J. Li, M. Tian,

J. Lin, B. Van der Bruggen, Elevated Performance of Thin Film Nanocomposite Membranes Enabled by Modified Hydrophilic MOFs for Nanofiltration, ACS Appl. Mater. Interfaces 9(2) (2017) 1975-1986. https://doi.org/10.1021/acsami.6b14412.

[44] S. Gao, Y. Zhu, Y. Gong, Z. Wang, W. Fang, J. Jin, Ultrathin Polyamide Nanofiltration Membrane Fabricated on Brush-Painted Single-Walled Carbon Nanotube Network Support for Ion Sieving, ACS Nano 13(5) (2019) 5278-5290. https://doi.org/10.1021/acsnano.8b09761.

[45] J. Wang, Y. Wang, J. Zhu, Y. Zhang, J. Liu, B. Van der Bruggen, Construction of TiO_2 @graphene oxide incorporated antifouling nanofiltration membrane with elevated filtration performance, J. Membr. Sci. 533 (2017) 279-288. https://doi.org/10.1016/j.memsci.2017.03.040.

[46] Y. Chen, F. Liu, Y. Wang, H. Lin, L. Han, A tight nanofiltration membrane with multi-charged nanofilms for high rejection to concentrated salts, J. Membr. Sci. 537 (2017) 407-415. https://doi.org/10.1016/j.memsci.2017.05.036.

[47] M.B.M.Y. Ang, Y.-L. Ji, S.-H. Huang, H.-A. Tsai, W.-S. Hung, C.-C. Hu, K.-R. Lee, J.-Y. Lai, Incorporation of carboxylic monoamines into thin-film composite polyamide membranes to enhance nanofiltration performance, J. Membr. Sci. 539 (2017) 52-64. https://doi.org/10.1016/j.memsci.2017.05.062.

[48] X. Yang, Y. Du, X. Zhang, A. He, Z. K. Xu, Nanofiltration membrane with a Mussel-Inspired Interlayer for improved permeation performance, Lamguir 33 (2017) 2318-2324. https://doi.org/10.1021/acs.langmuir.6b04465

[49] J. Zhu, S. Yuan, A. Uliana, J. Hou, J. Li, X. Li, M. Tian, Y. Chen, A. Volodin, B.V.

der Bruggen, High-flux thin film composite membranes for nanofiltration mediated by a rapid co-deposition of polydopamine/piperazine, J. Membr. Sci. 554 (2018) 97-108. https://doi.org/10.1016/j.memsci.2018.03.004.

[50] R. Zhang, S. Yu, W. Shi, W. Wang, X. Wang, Z. Zhang, L. Li, B. Zhang, X. Bao, A novel polyesteramide thin film composite nanofiltration membrane prepared by interfacial polymerization of serinol and trimesoyl chloride (TMC) catalyzed by 4-dimethylaminopyridine (DMAP), J. Membr. Sci. 542 (2017) 68-80. https://doi.org/10.1016/j.memsci.2017.07.054.

[51] F. Baskoro, C.-B. Wong, S.R. Kumar, C.-W. Chang, C.-H. Chen, D.W. Chen, S.J. Lue, Graphene oxide-cation interaction: Inter-layer spacing and zeta potential changes in response to various salt solutions, J. Membr. Sci. 554 (2018) 253-263. https://doi.org/10.1016/j.memsci.2018.03.006.

[52] C.-C. Ye, F.-Y. Zhao, J.-K. Wu, X.-D. Weng, P.-Y. Zheng, Y.-F. Mi, Q.-F. An, C.-J. Gao, Sulfated polyelectrolyte complex nanoparticles structured nanoflitration membrane for dye desalination, Chem. Eng. J. 307 (2017) 526-536. https://doi.org/10.1016/j.cej.2016.08.122.

[53] G.S. Lai, W.J. Lau, P.S. Goh, A.F. Ismail, Y.H. Tan, C.Y. Chong, R. Krause-Rehberg, S. Awad, Tailor-made thin film nanocomposite membrane incorporated with graphene oxide using novel interfacial polymerization technique for enhanced water separation, Chem. Eng. J. 344 (2018) 524-534. https://doi.org/10.1016/j.cej.2018.03.116.

[54] Y. Chen, C. He, High salt permeation nanofiltration membranes based on NMG-

assisted polydopamine coating for dye/salt fractionation, Desalination 413 (2017) 29-39. https://doi.org/10.1016/j.desal.2017.03.008.

[55] S. Ilyas, S.M. Abtahi, N. Akkilic, H.D.W. Roesink, W.M. de Vos, Weak polyelectrolyte multilayers as tunable separation layers for micro-pollutant removal by hollow fiber nanofiltration membranes, J. Membr. Sci. 537 (2017) 220-228. https://doi.org/10.1016/j.memsci.2017.05.027.

[56] W. Ding, H. Zhuo, M. Bao, Y. Li, J. Lu, Fabrication of organic-inorganic nanofiltration membrane using ordered stacking SiO_2 thin film as rejection layer assisted with layer-by-layer method, Chem. Eng. J. 330 (2017) 337-344. https://doi.org/10.1016/j.cej.2017.07.159.

[57] X. You, T. Ma, Y. Su, H. Wu, M. Wu, H. Cai, G. Sun, Z. Jiang, Enhancing the permeation flux and antifouling performance of polyamide nanofiltration membrane by incorporation of PEG-POSS nanoparticles, J. Membr. Sci. 540 (2017) 454-463. https://doi.org/10.1016/j.memsci.2017.06.084.

[58] Y.-L. Ji, Q.-F. An, X.-D. Weng, W.-S. Hung, K.-R. Lee, C.-J. Gao, Microstructure and performance of zwitterionic polymeric nanoparticle/polyamide thin-film nanocomposite membranes for salts/organics separation, J. Membr. Sci. 548 (2018) 559-571. https://doi.org/10.1016/j.memsci.2017.11.057.

[59] Q. Xie, W. Shao, S. Zhang, Z. Hong, Q. Wang, B. Zeng, Enhancing the performance of thin-film nanocomposite nanofiltration membranes using MAH-modified GO nanosheets, RSC Adv. 7(86) (2017) 54898-54910. https://doi.org/10.1039/c7ra11550d.

[60] M. Wu, T. Ma, Y. Su, H. Wu, X. You, Z. Jiang, R. Kasher, Fabrication of composite nanofiltration membrane by incorporating attapulgite nanorods during interfacial polymerization for high water flux and antifouling property, J. Membr. Sci. 544 (2017) 79-87. https://doi.org/10.1016/j.memsci.2017.09.016.

[61] Q. Shi, L. Ni, Y. Zhang, X. Feng, Q. Chang, J. Meng, Poly(p-phenylene terephthamide) embedded in a polysulfone as the substrate for improving compaction resistance and adhesion of a thin film composite polyamide membrane, J. Mater. Chem. A 5(26) (2017) 13610-13624. https://doi.org/10.1039/c7ta02552a.

[62] D. Qin, G. Huang, D. Terada, H. Jiang, M.M. Ito, A. H. Gibbons, R. Igarashi, D. Yamaguchi, M. Shirakawa, E. Sivaniah, B. Ghalei, Nanodiamond mediated interfacial polymerization for high performance nanofiltration membrane, J. Membr. Sci. 603 (2020) 118003. https://doi.org/10.1016/j.memsci.2020.118003.

[63] H.-Z. Zhang, Z.-L. Xu, Y.-J. Tang, H. Ding, Highly chlorine-tolerant performance of three-channel capillary nanofiltration membrane with inner skin layer, J. Membr. Sci. 527 (2017) 111-120. https://doi.org/10.1016/j.memsci.2016.12.059.

[64] Z. Yang, H. Guo, C.Y. Tang, The upper bound of thin-film composite (TFC) polyamide membranes for desalination, J. Membr. Sci. 590 (2019) 117297. https://doi.org/10.1016/j.memsci.2019.117297.